International Journal of Heat and Fluid Flow 82 (2020) 108532

Contents lists available at ScienceDirect

International Journal of Heat and Fluid Flow

journal homepage: www.elsevier.com/locate/ijhff

# Mixing characteristics of a film-exciting flapping jet

M. Wu[a], M. Xu[b], J. Mi[a,b,*], R.C. Deo[c]

[a] College of Engineering, Peking University, Beijing, 100871, China
[b] College of Marine Engineering, Dalian Maritime University, Dalian, 116026, China
[c] School of Agricultural Computational and Environmental Sciences, University of Southern Queensland, Springfield, QLD 4300, Australia

ARTICLE INFO

*Keywords:*
Film flutter
Flapping jet
Self-excited nozzle
Turbulent mixing

ABSTRACT

We have recently discovered a new type of self-excited flapping jets due to a flexible film whose leading edge is fixed at the nozzle exit [*Exp Ther Fluid Sci*, **106**, 226-233]. This paper is to report the experimental investigation on mixing characteristics of the jet induced by a rectangular FEP film. Hot wire anemometry and flow visualization are used to examine the flapping jet flow versus the non-flapping counterpart. Experiments are conducted under the following conditions: i.e., $L/D = 1.0$ (fixed), $W/D = 0.03 \sim 1.0$ (varying) and $Re = 10000 \sim 45000$ (varying); where $W$ and $L$ are the film's width and length, $D$ is the nozzle-exit diameter, and $Re$ is the Reynolds number defined by $Re \equiv U_o D/\nu$ with $U_o$ and $\nu$ being the jet-exit velocity and fluid viscosity.

It is found that the jet-flapping frequency $f_F$ varies with $W$ in a complex fashion while it grows roughly linearly with increasing $U_o$ for $W/D \geq 0.5$. The flapping Strouhal number $St_F \equiv f_F D/U_o$ ranges in $0.13 \leq St_F \leq 0.23$ for $Re = 15{,}000 \sim 45{,}000$. These Strouhal numbers are substantially lower than that ($\approx 0.45 \sim 0.7$) for the primary vortex generation in the free jet, but one to two orders of magnitude higher than those from the conventional self-exciting fluidic devices. In general, the flapping jet decays and spreads more rapidly than does the free jet. As $W$ increases, the decaying and spreading rates both grow. Of significance, the centerline evolutions of Taylor and Kolmogorov scales versus the integral scale are examined to characterize the small scales of turbulence against the large-scale motion.

## 1. Introduction

Turbulent jets are typical flows in both nature and industry. Robust control of jet mixing is essential to optimize any industrial nozzle's performance. Significant efforts have been dedicated to the development of controllable mixing nozzles. In the aeronautical sector, for example, an oft-stated aim to increase combustion intensity or reduce flame volume is to increase the mixing rates between the jet and coflow. These nozzles are classically designed to excite the coherent large-scale motions embedded in the shear layer of an emerging jet, because such motions play a dominant role in the gross transport of mass and momentum in jets and jet flames (Mungal et al., 1991). Both active and passive controls of turbulent jets were extensively investigated by experiment to achieve the "enhanced mixing" of turbulent jets, especially, during the 1970-1990s. Popular approaches of active excitation were, e.g., acoustic excitation (e.g., Crow and Champagne, 1971; Parekh et al., 1983; Reynolds et al., 2003) and mechanical excitation involving moving parts (e.g., Simmons et al., 1981; Davis, 1982). Acoustic excitation of jets is typically achieved with loudspeakers inside the nozzle to increase the coherence and intensity of the large-scale motions using the natural coupling of flow instabilities and acoustic resonances (e.g., Hill and Green, 1977). This excitation nevertheless requires high-intensity, narrow-band acoustic energy at frequencies that are within the audible spectrum. For example, bifurcating and blooming jets can be successfully forced in laboratory at low Reynolds numbers ($Re < 10^4$) but require much stronger forcing at high Reynolds (Reynolds et al., 2003). Another approach to enhance jet mixing is the use of mechanically oscillating nozzles (e.g. Simmons et al., 1981). In addition, active controls of jet mixing were later very successfully studied by numerical simulations (e.g., Gutmark and Grinstein, 1999; Danaila and Boersma, 2000; Silva and Metais, 2002; Tyliszczak and Geurts, 2014; Gohil et al., 2015; Tyliszczak, 2015). It is worth noting that the active devices are generally utilized to stimulate large-scale pulsations, oscillations or flapping of the entire jet in the near field.

The active excitation techniques were proved quite effective in laboratory studies but much less feasible and effective in practical applications, e.g., for combustion in furnace under harsh conditions, due to their complexity of system, weight, power and maintenance requirements. Although (Reynolds et al., 2003) mentioned a

* Corresponding author at: Peking University, College of Engineering, Beijing 100871, China.
*E-mail address:* jmi@pku.edu.cn (J. Mi).

https://doi.org/10.1016/j.ijheatfluidflow.2019.108532
Received 17 August 2019; Received in revised form 21 November 2019; Accepted 26 December 2019

demonstration of active flow control on an aircraft engine by Glauser and Walker (1998) and Kibens et al. (1999), to our best knowledge, no industrial burners have been reported to effectively operate using any of active control methods. For practical applications, the excitation technique should be simple and effective with no moving components. In this context, several types of practical self-exciting nozzles were developed for the enhancement of jet mixing, such as the flip-flop jet (Viets, 1975; Mi et al., 2001), precessing jet (Nathan and Luxton, 1991), oscillating jet (Mi et al., 1998; Nathan et al., 2006) and the "whistler" nozzles (Hill and Greene, 1977). These "passive-control" devices naturally excite the jet itself into time-dependent self-oscillation. It has been recognized that such a dynamic self-excited oscillation significantly increases the large-scale mixing of the jet and so benefits for some practical processes. The self-exciting nozzles have found various industrial applications (e.g., Manias and Nathan, 1993). Also, several fundamental studies have been performed for the self-excited jet oscillation (e.g., Raman and Cornelius, 1995; Xu et al., 2012).

However, the above passive self-exciting nozzles commonly cause a significant loss of pressure (energy) during their operation. This pressure loss is local and mainly due to sudden expansion and/or contraction that the fluid flows through. To avoid this loss, Xu et al. (2019) have developed a new type of flapping jets that are self-excited by the flutter of a flexible film at a round nozzle exit, which has substantially lower pressure-loss due to the film flutter. Their experiments revealed that a thin and light film, when being placed centrally along the nozzle axis, often flutters periodically under sufficiently strong airflow. The flutter frequency increases as either the film length decreases or the jet velocity rises. Importantly, the flutter domain was found to reduce with increasing the film stiffness and varies with the film shape, size and thickness. It was also demonstrated that the flapping jet evolves downstream with much higher spreading and decaying rates versus the non-flapping free jet. And this evolution was enhanced as the film length was increased. However, Xu et al. (2019) have not yet characterized the turbulent mixing of the flapping jet to any extent. To fill this gap, the present work is designated to investigate by experiment the mixing characteristics of the flapping jets under varying film width versus a free circular jet from the same nozzle. Toward this end, not only the flow visualization is taken but also the instantaneous velocity along the jet centerline is measured using hot-wire anemometry so as to provide various statistical data, including the mean and RMS (root-mean-squared) velocities, as well as the turbulent length scales.

## 2. Experimental details

### 2.1. Experimental setup

The present experimental study used the facilities shown in Fig. 1. Namely, we utilized a smoothly contracting round nozzle of $D = 40$ mm the exit diameter, to which various films can be attached, whose schematic with a film and an oscillating jet is also displayed. A LabVIEW-based computer was used to control the frequency converter, so the blower voltage, and the blower to produce an airflow with a prescribed flow rate or a jet speed. The blower outlet is attached to a 1.5 m long rectifier box. The rectifier box is equipped with a honeycomb grid and a metal grid. In hot-wire measurements, the probe was positioned through the three-dimensional coordinate frame and control system. The origin of the $(x,y,z)$ coordinates was chosen to be the center of the nozzle exit; namely, $x$ is the downstream distance measured from the nozzle exit and $y$ is the lateral distance from the centreline and perpendicular to the film span or width. The choice of this coordinate system resulted in both the flapping and non-flapping (free) jets having the identical initial conditions. Of note, the film flaps predominantly in the $y$ direction. The $x$ range of measurements is $x/D = 0$-23.

Six different-width films of fluorinated ethylene propylene (FEP) at the thickness of $\delta = 50$ μm were selected for this study; the widths are $W/D = 0.03$, 0.125, 0.25, 0.5, 0.75 and 1.0. A clip of axisymmetric airfoil profile (see Fig. 1) of PLA material with the maximal thickness of 1.0 mm was used to fix the film with double-sided tape. To keep the stress equally on both sides as much as possible, the film was clamped highly carefully by the clip. Note that, apart from the pressure loss, the excessive thickness of the clip may generate small vortices and then affect the film flutter, so the whole clip size was chosen as small as possible.

### 2.2. Flow visualization

To identify the flapping motion, a great number of instantaneous flow images of a smoked jet were taken by a Canon camera (EOS 5D Mark iii) equipped with the focal length 24 ~ 105 mm. The smoking was realized through a fog machine whose spray volume is 11.8 $m^3/s$ with a nozzle diameter of 1.0 mm. The mixing between the working fluid and the seeding fog took place in a reservoir located upstream of the stagnation chamber. The evergreen light source is class IV laser product for applications (532 nm wavelength, <10 W peak power) with an exit beam diameter of about 8 mm and the exit angle of 90 degrees. The track of the laser volume was parallel to the $xy$ plane with the illuminated region extending for about 1000 mm along the $x$ direction and for about 500 mm along the $y$ direction.

### 2.3. Hot-wire anemometry

The instantaneous streamwise velocity component on the centerline was measured using hot-wire anemometry. The measuring probe consisted of a single tungsten wire of 5 μm diameter with an active length of approximately 1 mm, normal to the streamwise ($x$) direction. The wire was operated by an in-house constant temperature circuit at an over-heat ratio of 1.5. The signals through the circuit were offset, amplified and then digitized by a personal computer with a 12-bit A/D converter, at a sampling frequency of 50 kHz and a record duration of 120 seconds. The hot wire was calibrated against a miniature standard pitot tube in the low-turbulence (≈ 0.6%) unmixed core of the jet from the smoothly contracting circular nozzle. Calibrations were performed before and after each set of measurements. Third polynomial curves were used to fit the calibration data, i.e., $U = a_0 + a_1E + a_2E^2 + a_3E^3$; here, $E$ is the voltage over the hot-wire placed in the stream at a given velocity $U$ measured by the pitot tube, while constants $a_i$ ($i = 1$~3) were determined by varying 6 to 10 values of $U$.

The hot-wire probe had a limited resolution due to its finite spatial dimensions and temporal response. Specifically, its resolution was determined by the wire diameter $d_w = 5$ μm and effective length $\ell_w \approx 1.0$ mm, plus its response frequency and sampling rate during measurements. Note that the ratio $\ell_w/d_w \approx 200$ is required so that both a nearly uniform temperature distribution in the central portion of the wire and a high sensitivity to flow velocity fluctuations can be achieved. The present study corrected the spatial attenuation of the single wire due to $\ell_w \approx 1$ mm using the procedure of Wyngaard (1968), which was developed in spectral space to account for the integration effect on Fourier components of the velocity.

To properly estimate the Taylor and Kolmogorov scales (λ, η), the present study utilized the digital scheme of filtering high-frequency noise developed by Mi et al. (2005) to remove the high frequency noise. This scheme obtained the 'true' values of the Kolmogorov scales $\eta$ and $f_K$ by filtering the measured velocity signal $u(t)$ and calculating the dissipation rate $<\varepsilon>$ from $u(t)$, using the isotropic relation $<\varepsilon> = 15\nu <(\partial u/\partial x)^2>$ together with modified Taylor's hypothesis $\partial u/\partial x = (U_c+u)^{-1}\partial u/\partial t$, rather than $U_c^{-1}\partial u/\partial t$.

## 3. Results and discussion

### 3.1. Film flutter characteristics versus W and Re

Once a fluid flows sufficiently rapidly over a film of finite, but too narrow, width ($W$), the film flutter will occur due to aerodynamic

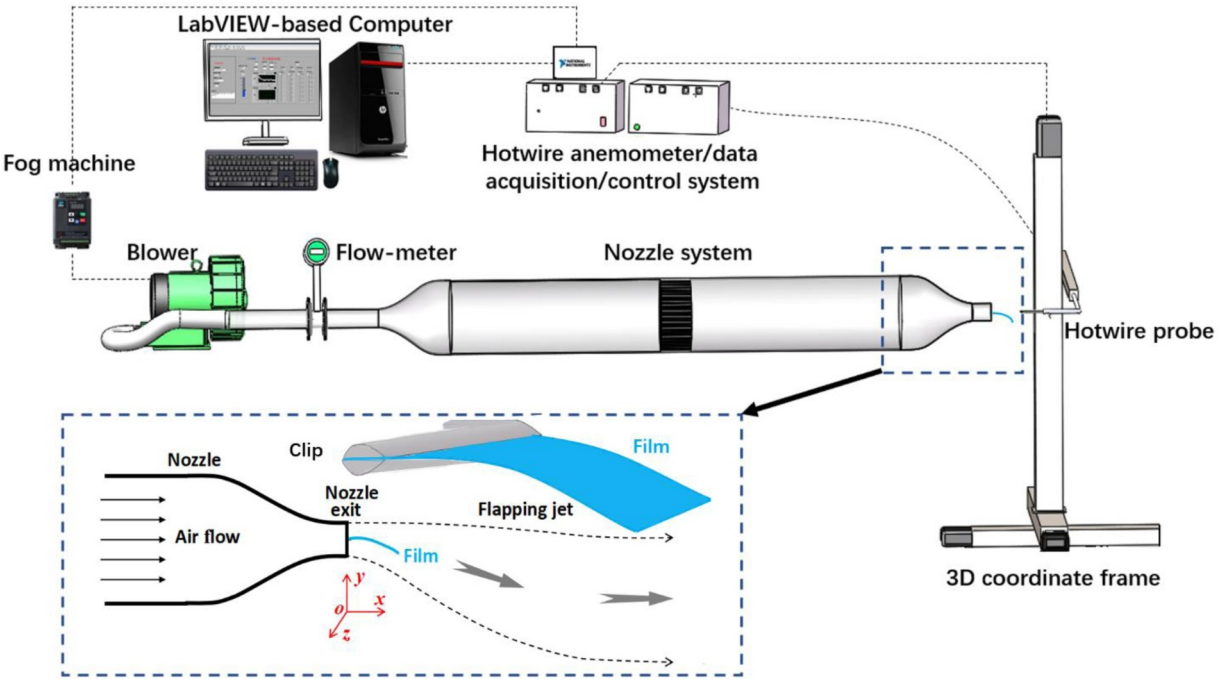


**Fig. 1.** Experimental facilities and schematic of a smooth contraction nozzle with a film and a flapping jet, together with the coordinate system.

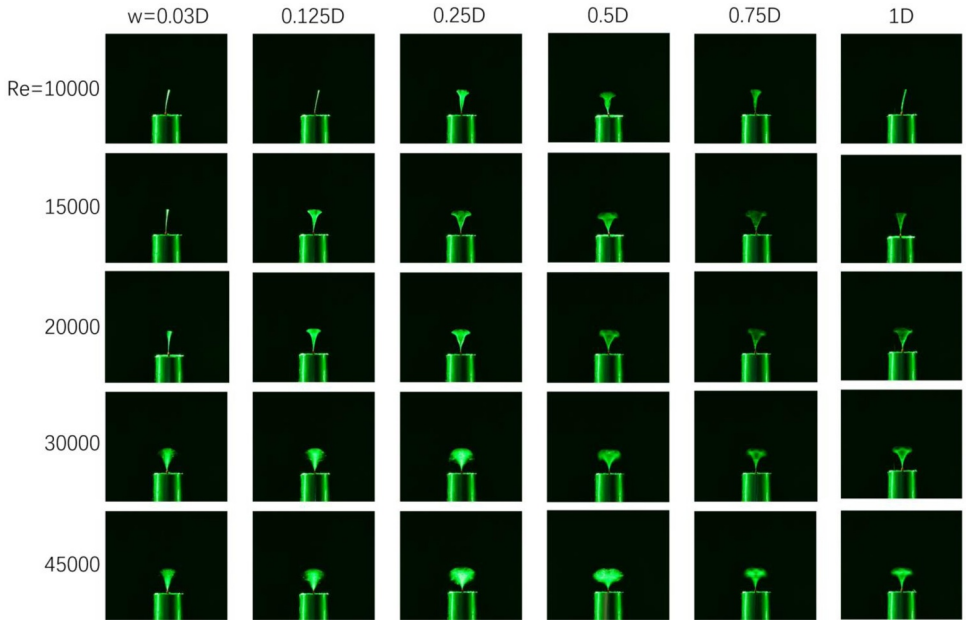


**Fig. 2.** Long-exposure (20 s) photographs of varying-width FEP films of $L/D = 1$, in the flapping plane, fixed at the nozzle exit for $Re = 10000$ to 45000 and $W/D = 0.03$ to 1.0 as indicated.

instability (see Païdoussis, 2016). Similarly, when a fluid jet issues from a nozzle and flows over a film fixed axially at the nozzle exit, the film is expected to flutter as the jet speed or Reynolds number ($Re$) is high enough, thus exciting the jet itself to flap. The film flutter is expected to be quasi-periodic, and its frequency ($f_F$) should be dependent upon $W$ and $Re$. Fig. 2 displays the long-exposed (20 s) photographs of different films of $W/D = 0.03$ to 1.0 and $L/D = 1$, whose leading end was fixed at the nozzle exit; the corresponding jets operated at $Re = 10000 \sim 45000$ as indicated on the plot. A close look can find that the film flutter did not happen only in the following five cases, i.e. $W/D = 0.03$ and $Re = 10000$, 15000 & 20000; $W/D = 0.125$ and $Re = 10000$; and $W/D = 1.0$ and $Re = 10000$. These observations imply that both $W$ and $Re$ have significant impact on the occurrence of film flutter. In particular, the probability of flutter reduces as $W$ is decreased. It is highly likely to have no flutter when the film becomes a filament even at very high $Re$.

Careful inspections to Fig. 2 suggest that the amplitude of film flutter depend strongly on the film width ($W$) and Reynolds number ($Re$). To demonstrate this dependence more quantitatively, Fig. 3 shows the relative amplitude ($A/D$) versus $Re$ for different $W$. Obviously, for all $W$, $A$ grows generally as $Re$ increases. However, the $A$-$Re$ relationship appears to be complex and varies significantly with $W$. The reason behind is highly likely associated with a large variation of three-dimensionality with changing $W$. The thinner is the film width ($W$), the higher is the three-dimensionality, hence the more complex is the $A$-$Re$ relationship. Nonetheless, the detailed analysis on such an issue is obviously out of the scope of this study and hence left for a study in future

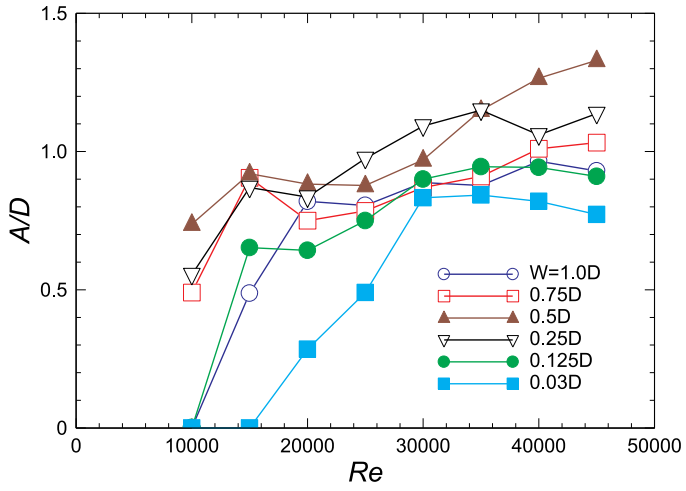


**Fig. 3.** Amplitude ($A$) of the film flutter versus $Re$ for different film widths ($W$).

(if necessary).

In general, the film flutter can induce the jet to flap globally, thus suggesting that the flutter frequency ($f_F$) must be equal to the flapping frequency. Also, the jet flapping should be someway periodic since the previous experiments (see Païdoussis, 2016) well revealed the periodicity of the film flutter in the wind tunnel. It follows that we can measure $f_F$ through measuring the power spectra ($\Phi_u$) of the fluctuating velocity ($u$). Fig. 4 indeed provides a support for this. It shows the frequency distributions of $\Phi_u$ obtained at $x/D = 1.2$ and $r/D = 0.5$ in a free jet (removing the film) and different-$W$ flapping jets at $L = D$ and $Re = 30000$. Evidently, the periodic flutter is clearly reflected in $\Phi_u$ for $W/D \geq 0.125$. The first or primary spike seen in $\Phi_u$ corresponds to the film flutter or jet flapping frequency $f_F$. This frequency is lower than the naturally shedding frequency ($f_N$) of the primary vortex of the free jet, which is roughly identified by the very broad peak in $\Phi_u$. Moreover, a detailed check can make two significant observations:

(1) As $W$ is increased, the frequency for the first spike, i.e., $f_F$, increases and then reduces slightly but discernibly;
(2) As $W$ is increased, the harmonic spikes in $\Phi_u$ increase in number and can be better defined, indicating an increased periodicity of the flapping.

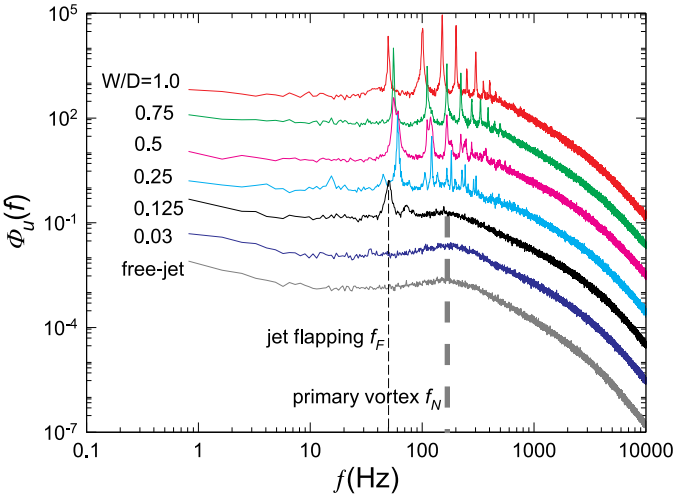


**Fig. 4.** Power spectra ($\Phi_u$) of the fluctuating velocity $u$ in the jet at $x/D = 1.25$ and $r/D = 0.5$ for different indicated widths of the film at $L = D$ and $Re = 30000$.

The first observation has been validated by several independent measurements. The second one is anticipated because the two-dimensionality of the film flutter is enhanced by widening the film, which consequently improves the flapping periodicity. A better periodicity surely results in more harmonics in the frequency spectrum.

Fig. 5(a) displays $f_F$ versus $Re$ for different $W$ at $L = D$. It is clearly demonstrated that $f_F$ rises with increasing $Re$. Of note, the measured relationship of $f_F$ versus $Re$ is well linearized for $W/D \geq 0.50$, as indicated with lines on the plot. However, this linearity does not hold for the narrower films at $W/D < 0.50$ perhaps due to the complex three-dimensionality of their flapping. Also, evidently, the growth rate of $f_F$ with $Re$ is substantially higher for $W/D \geq 0.50$ than for $W/D < 0.50$. This difference is reflected in the mixing characteristics of the flapping jet reported later in Figs. 7–10. The jet flapping motion should occur in a lessened area and so become more three-dimensional as the film width reduces or the aspect ratio $W/L$ is decreased. Besides, for any $Re$, as $W$ increases from $0.125D$ to $1.0D$, $f_F$ rises first and then drops, with the highest value of $f_F$ always occurring at $W/D = 0.5$.

Fig. 5(b) shows the dimensionless flapping frequency, i.e., the flapping Strouhal number defined by $St_F \equiv f_F D/U_o$ against $Re$. Obviously, $St_F$ does not vary greatly with $Re$ for $W/D \geq 0.50$ and ranges between 0.13 and 0.23. The change of $St_F$ owing to $W$ is like that of $f_F$ because the same length scale (i.e., $D$) is used for the normalization. Of note, the flapping $St_F$ is much smaller than the Strouhal number $St_N$ ($\approx 0.45 \sim 0.7$) for the natural instability of the free jet.

### 3.2. Mixing characteristics of the flapping jet

The film flutter causes the jet to flap, which can be visualized by smoking the jet. To visually explore the influence of the film width ($W$), Fig. 6 shows the smoked jet images taken for $W = 0.125 \sim 1.0D$ and $L = 1.0D$ at $Re = 30000$. Note that the right and left panels of images in both Fig. 5(a) and (b) are for the instantaneous and mean jets, respectively. It is observed straightforwardly that, as $W$ is increased, the spread rate of the flapping jet grows rapidly in the flapping plane, especially from $W/D = 0.125$ to $W/D = 0.5$. However, the spread rate in the bisecting plane changes little relative to the free-jet case. These observations suggest undoubtedly that the flapping jet should have substantially greater large-scale mixing than does the free jet. As a result, the former decays faster than the latter (Fig. 7). It is also expected that the decay rate should increase as $W$ is increased. This can be approved below by the measurement of the centerline mean velocity.

Fig. 7 presents the centreline mean velocity in the form of $U_o/U_c$ versus $x/D$, where $U_c$ and $U_o$ are the local centerline mean velocity and its exit value, respectively, for various film widths at $Re = 30{,}000$. For reference, the present free-jet result at $Re = 30000$ and that of Mi and

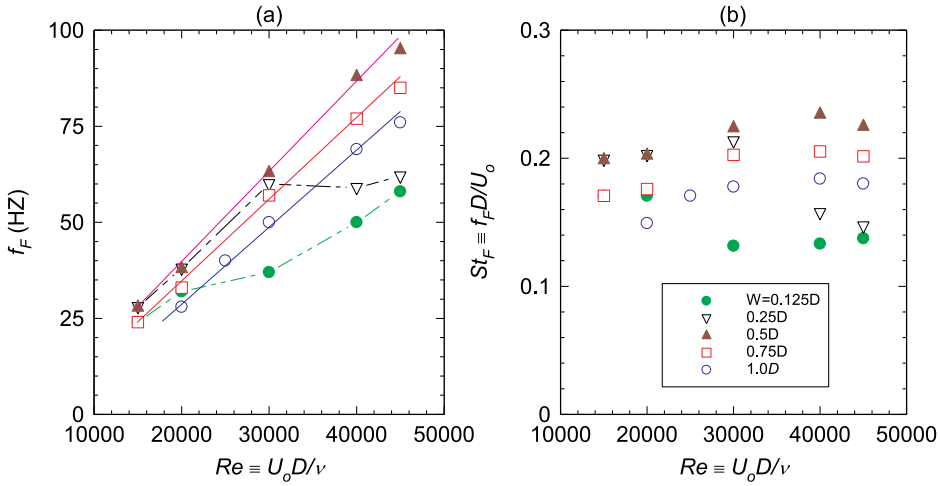


**Fig. 5.** (a) Jet-oscillating frequency $f_F$ and (b) Strouhal number $St_F$ versus the jet-exit Reynolds number $Re$ for different film widths at $L = D$.

Nathan (2010) obtained at $Re = 15{,}000$ are also given. Notably, a good agreement is demonstrated between our $U_o/U_c$ and that of Mi and Nathan (2010) for the free jet, thus crediting the present hot-wire measurements. It is evident on the plot that the flapping jets all have a higher growth rate of $U_o/U_c$ than the free jet. That is, the flapping jet decays generally at a higher rate, which coincides with a higher spread rate in the flapping plane (see Fig. 6). Moreover, another observation can be made from Fig. 7 that the decay rate of the flapping jet increases as the film widens. Particularly, the ratio $U_o/U_c$ for all the cases increases well linearly with $x$ for $x/D \geq$ 8-10; i.e., $U_o/U_c \propto K(x/D)$, where the slope $K$ represents the decay rate of $U_c$ or the jet. To display the decay rate more clearly, an inset for $K$ versus $W/D$ is plotted in Fig. 7. It is interesting to note that the linearization of $K \propto W$ is violated at $W = 0.5D$. In other words, the decay rate of the flapping jet rises doubly when the film is widened from $W = 0.25D$ to $W = 0.5D$. This observation is noticeably in line with that from Fig. 6 which compares the spreading widths of the different smoked jets. It also coincides indirectly with the strong $W$-dependent variation of the flapping frequency versus $Re$ in Fig. 5(a), as well as the $W$-dependent behaviors of the centerline turbulence intensity reported below in Fig. 8.

To characterize the large-scale turbulent mixing, Fig. 8 shows the relative turbulence intensity defined by the ratio $<u^2_c>^{1/2}/U_c$ along the jet centreline for $Re = 30000$ at $L = D$ and varying $W$. For comparison, the free-jet result of Mi and Nathan (2010) for $Re = 15000$ is reproduced on the plot. Note that the ratio $<u^2_c>^{1/2}/U_c$ appears to have a process of first decreasing and then increasing at $x/D < 3$ for all the cases except from $W/D = 0.5$. This is likely due to the film flutter right upstream at $x/D = 0{\sim}1.0$, causing the ratio to behave so. Nevertheless, it is believed that such an unwanted matter has little impact on the downstream variation of $<u^2_c>^{1/2}/U_c$.

Several observations can be made from Fig. 8. At first, the present turbulent intensity for the free jet is well compatible to that of Mi and Nathan (2010) over the whole range of $x/D$. Secondly, relative to the free jet, the flapping jet generally exhibits much stronger fluctuations and consequently a far higher ratio $<u^2_c>^{1/2}/U_c$ due to the large-scale flapping in the region at $x/D < 12$. Thirdly, for the cases of $W/D \geq 0.5$,

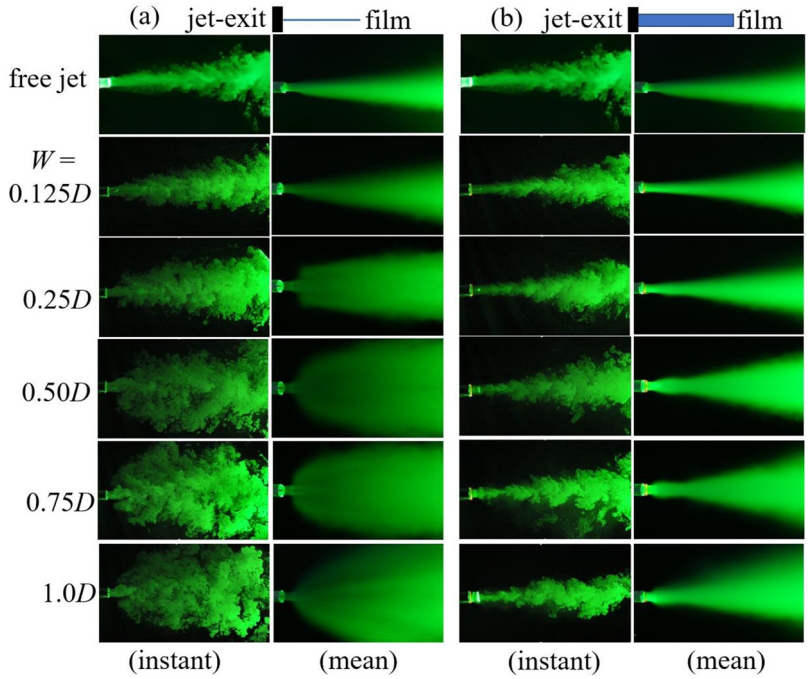


**Fig. 6.** Images of the smoked jets, in (a) the flapping plane and (b) the bisecting plane, from the nozzle exit with the film width $W = 0.125D \sim 1.0D$ and length $L = D$ versus the free jet ($L = 0$) at $Re = 30000$.

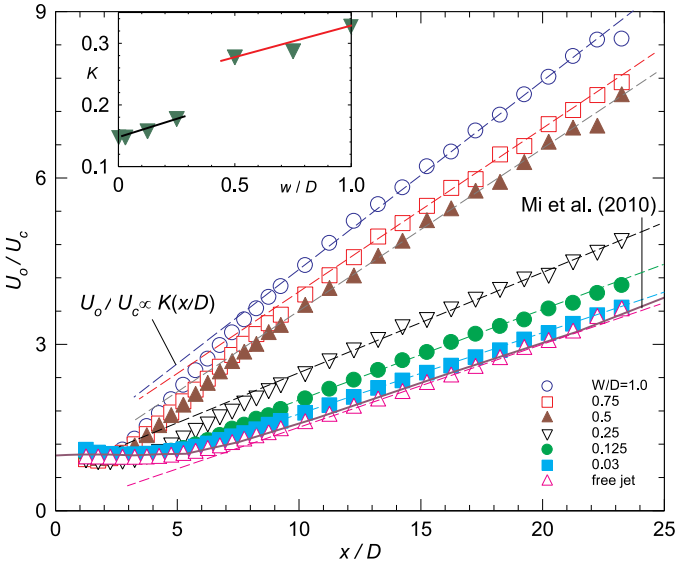


**Fig. 7.** Centreline velocity decay $U_o/U_c$ versus $x/D$ at $Re = 30000$ for different widths of the film at $L = D$. The inset illustrates the decay rate $K$ versus $w/D$.

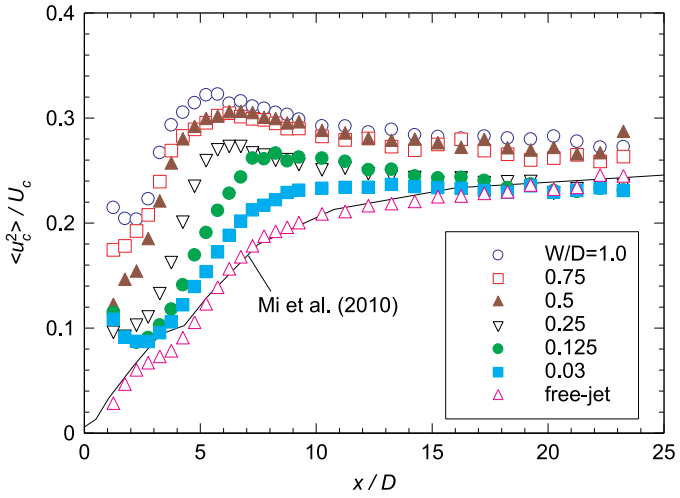


**Fig. 8.** Turbulence intensity defined by $<u^2_c>^{1/2}/U_c$ along the jet centreline at $Re = 30{,}000$ for different widths of the film at $L = D$.

as the flow proceeds downstream, the ratio $<u^2_c>^{1/2}/U_c$ initially grows, then turns to decrease around $x/D = 5$, and, farther downstream, gradually narrows its gap from the free jet but maintains to be significantly higher. Furthermore, for all $W/D \geq 0.5$, the centerline variation of $<u^2_c>^{1/2}/U_c$ is nearly the same, in particular, at $x/D > 6$, and its magnitude is considerably higher than that for $W/D < 0.5$. However, for the flapping jet at $W/D < 0.5$, the ratio $<u^2_c>^{1/2}/U_c$ becomes nearly identical with that for the free jet at $x/D \geq 18$, despite a large difference initially.

The above observations may be explained here. When the film is not wide enough at $W/D < 0.5$, its flutter can induce only a small amount of fluid to oscillate in a narrow region, so unable to cause a large-scale mixing across the jet. Consequently, the flapping-related velocity fluctuation along the centerline or the contribution to $<u^2_c>^{1/2}/U_c$ from the upstream flapping decays fast and vanishes downstream at $x/D >$ 18-20. For $W/D \geq 0.5$, the film is sufficiently wide and so its flutter can strongly stir the jet flow, resulting in large velocity fluctuations which can sustain over a long downstream distance.

Note that the turbulence intensity represents the degree at which the turbulent mixing occurs at the large scales of turbulent fluctuation. So, Fig. 8 suggests that the flapping jet generally has a greater large-scale mixing than the non-flapping free jet, especially, in the near field at $x/D < 10$. In other words, the film flutter plays a significant role in enhancing the large-scale mixing of fluid in the jet flow.

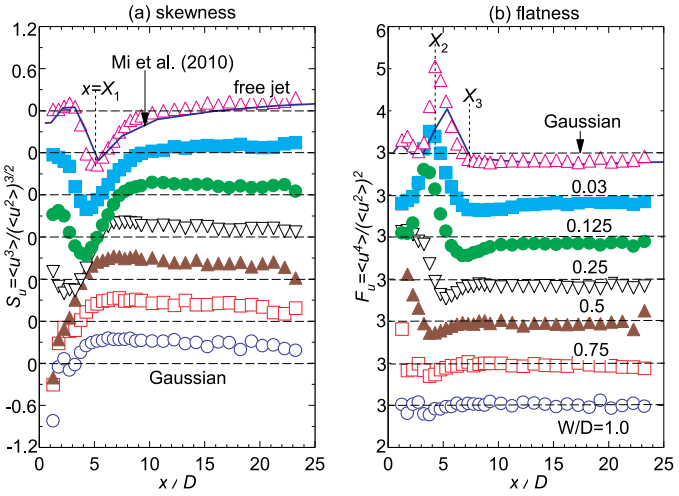


**Fig. 9.** Centreline evolutions of (a) the skewness $S_u$ and (b) the flatness $F_u$ in the jets at $Re = 30{,}000$ for different widths of the film at $L = D$.

The turbulent mixedness of the original jet and ambient fluids may be embodied in the PDF of the fluctuating velocity ($u$) or simply reflected by the skewness and flatness factors of $u$, i.e., $S_u = <u^3>/<u^2>^{3/2}$ and $F_u = <u^4>/<u^2>^2$. The better fine-scale mixing corresponds to less departures of these factors from their Gaussian values (0, 3) (e.g., Mi, 2006). Fig. 9(a) and (b) present the two factors $S_u$ and $F_u$ along the centerline for all the jets of investigation. For comparison, the free-jet result ($Re = 15{,}000$) of Mi and Nathan (2010) is also plotted. Broadly, the variations of both $S_u$ and $F_u$ are very roughly similar over the measured region for all the jets. However, both $S_u$ and $F_u$ evolve distinctly in the near field for different jets. Perhaps for all the jets, $S_u$ exhibits a dip at $x = X_1$ in the very near field whereas $F_u$ peaks at $x = X_2$, which is slightly smaller than $X_1$, and then hollows farther downstream at $x = X_3$. It is speculated that both $X_1$ and $X_2$ occur immediately downstream from or around the end of the unmixed (or sometime called 'potential') core of the jets. This was indicated in Mi and Nathan (2010) for the circular and noncircular free jets. Basically, there would be no ambient fluid to be entrained across the jet centerline at $x < X_1$. For $W/D > 0.25$, the sufficiently wide film can induce the entire jet to flap and thus 'drag' the ambient fluid to cross the center, so mixing the fluids from the nozzle exit and ambient, even at $x \leq L$ (film length) or $x/D \leq 1.0$, where no measurements were taken (so both $X_1$ and $X_2$ are not observed for $W/D > 0.25$). In contrast, the very narrow film cannot induce the entire jet to flap and drag the ambient fluid to cross the centerline, see Fig. 6. That is, in the cases of $W/D \leq$ 0.25, there is some unmixed fluid from the jet nozzle along the centerline at $1.0D \leq x < X_1$. In this sense, all the special positions of $X_1$, $X_2$ and $X_3$ should shift upstream as $W$ is increased, see Fig. 9. In addition, a note is worth making here on the special position of $X_1$ or $X_2$: they are deduced to be intermittently occupied by the high-velocity 'unmixed' primary nozzle fluid, the low-velocity 'unmixed' ambient fluid (entrained into the jet) and the 'mixed' fluid from within the mixing-layers, thus causing the probability density function (PDF) of $u$ to be highly skewed and significantly different from the Gaussian distribution; as a consequence, the values of $S_u$ and $F_u$ measured over there differ greatly from the Gaussian values (0, 3).

As the flow proceeds downstream at $x > X_3$, the distinctions in $S_u$ and particularly in $F_u$ between different jets tend to reduce gradually. For $W/D > 0.25$, as $x$ increases, $F_u$ reaches the Gaussian value (3.0) rapidly while $S_u$ first grows to exceed, and then decreases slowly but retains well above, the Gaussian value. Defiantly for $W/D < 0.25$, $S_u$

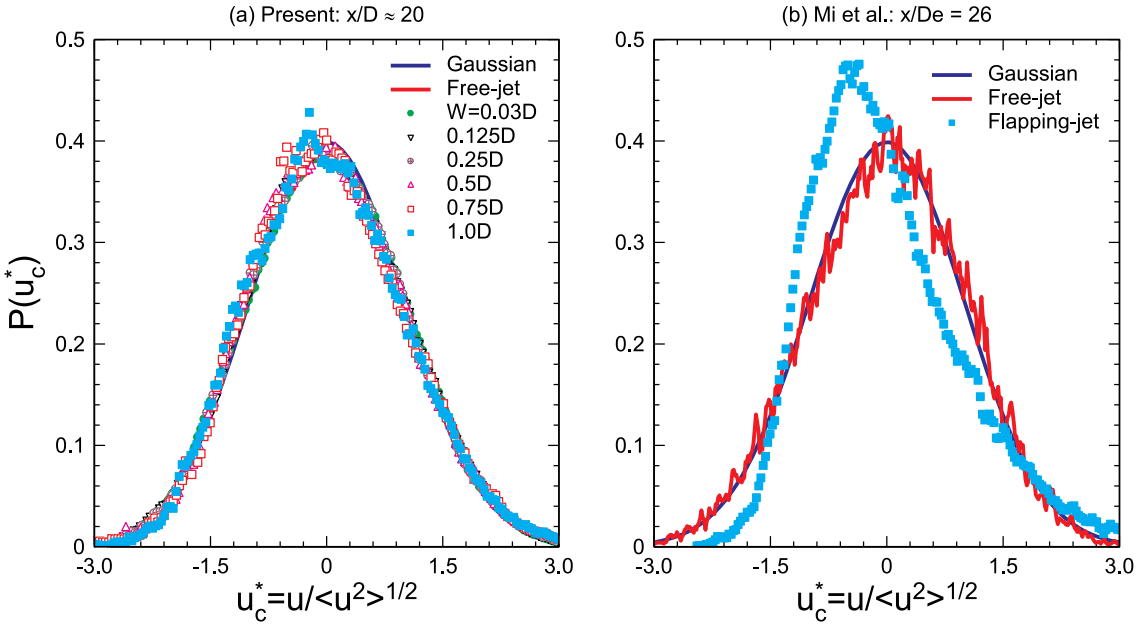


**Fig. 10.** Probability density function of the centerline fluctuating velocity ($u_c$), i.e., $P(u_c)$. (a) Present jets at $x/D \approx 20$ for $Re = 30000$; (b) the jets of Mi et al. (2001) at $x/D_e = 26$ for $Re = 15500$.

first rises and then maintains constantly ($> 0$) whereas $F_u$ quickly reaches a constant $< 3.0$ and then sustains at this value. Interestingly, as $W$ increases, both factors rise grossly at $x/D \geq$ 8-10, with $S_u$ deviating more, and $F_u$ differing less, from their Gaussian values. For the free jet, $S_u$ ($> 0$) keeps to grow slowly over the measurement range of $x/D$ and may never reach the asymptotic value while $F_u$ develops to be a constant below 3. To conclude, the centreline PDFs of all the jets (not presented) will never reach the Gaussian distribution, whose $S_u = 0$ and $F_u = 3$ simultaneously. This is because all the jets are open, into which the 'fresh' unmixed ambient fluid is continuously entrained.

Mi et al. (2001) revealed that the flapping motion from a fluidic nozzle acts to redistribute the turbulence kinetic energy by enhancing the large-scale mixing and simultaneously suppressing the generation of fine-scale turbulence. This is however unlikely to apply for the present flapping jets whose $St_F$ ($\approx 0.13 \sim 0.23$) is much higher than that ($\approx 2.8 \times 10^{-3}$) from their fluidic nozzle. It is postulated that the jet-flapping in the present cases should significantly enhance the turbulent mixing over both small and large scales. Some supporting evidence for this postulation is provided below.

Fig. 10(a) shows the probability density functions (PDFs) of the centreline fluctuating velocity $u$, $P(u_c)$, obtained at $x/D \approx 20$ in both the film-flapping jets and the free jet for $Re = 30000$. For comparison with Mi et al. (2001), Fig. 10(b) replots their PDF data for the flapping and non-flapping rectangular jets obtained at $Re = 15500$ and $x/D_e = 26$, where $D_e$ is the equivalent diameter of rectangular exit. For reference, the Gaussian distribution is also shown on the plots. Fig. 10(a) clearly demonstrates that $P(u)$ is closely Gaussian, suggesting well small-scale mixing, for all the present flapping jets and the free jet on the centerline at $x/D = 20$.

In contrast, the PDFs from the two jets of Mi et al. (2001) are very distinct. There is a significantly higher probability of the occurrence of low-velocity fluid in the flapping jet, as indicated by the steep drop on the left side of $P(u_c)$, than in the non-flapping jet. This indicates that there is a significant increase in the quantity of low-velocity, presumably unmixed ambient, fluid in the far-field flapping jet. This bias in low-velocity fluid can be expected to result from the occasional appearance on the centreline of the entrained, yet poorly-mixed fine-scale, fluid parcels induced by the upstream very slowly flapping motion. By contrast, for the non-flapping case, the flow is mixed much better at fine-scale or molecular levels in the central region at $x/D_e = 26$ and so $P(u)$ is nearly Gaussian. Note that $(S_u, F_u) = (0.87, 3.96)$ for the flapping jet of Mi et al. (2001) versus $(S_u, F_u) = (0.25, 2.93)$ for the present flapping jet with $W/D = 1.0$ and $(S_u, F_u) = (0, 3)$ for Gaussian.

### 3.3. Characteristic scales of turbulent mixing of the flapping jet

To characterize large, intermediate and small-scale turbulence structures, we obtained the integral ($\Gamma$), Taylor ($\lambda$) and Kolmogorov ($\eta$) scales using the traditional methods. That is, $\Gamma$ was approximately estimated from the integral time scale $T$, based on Taylor's frozen hypothesis, viz.,

$$\Gamma = U_c T = U_c \int_0^{\tau_0} \langle u(t)u(t+\tau)\rangle \langle u^2\rangle^{-1} d\tau, \tag{1}$$

where $\tau_0$ corresponds to the first zero crossing of the autocorrelation function $\langle u(t)u(t+\tau)\rangle$. The Kolmogorov scale $\eta = (\nu^3/\langle\varepsilon\rangle)^{1/4}$ was obtained by $\langle\varepsilon\rangle = 15\nu < (\partial u/\partial x)^2 >$, the isotropic-turbulence dissipation, and the Taylor scale was estimated by $\lambda = < u^2 >^{1/2} / < (\partial u/\partial x)^2 >^{1/2}$, where $\partial u/\partial x = (U_c + u)^{-1} \partial u/\partial t$. Fig. 10(a)–(c) respectively show the results of $\Gamma/D$, $\lambda/D$ and $\eta/D$ for $x/D \geq 6$. Note that these length scales for $x/D < 6$ were not estimated because both the spatial (hot-wire size) and temporal resolutions in the near field were insufficient for the appropriate calculations of $\partial u/\partial t$ and thus $\lambda$ and $\eta$. Like Figs. 7–10, Fig. 11(a-c) also present the results of Mi and Nathan (2010) for comparison.

For the circular free jet, $\Gamma$ represents the large-scale length, alike the mean-flow half-radius or diameter, and is thus expected to vary linearly with $x$ in the far-field self-preserving region. Apparently as seen in Fig. 11(a), $\Gamma$ increases very roughly linearly with $x$ for $x/D \geq 6$. This linearity also appears to apply for the flapping-jet cases. It is evident that the slope of the linearized $\Gamma \propto x$, i.e., the growth rate of $\Gamma$, rises as $W$ increases. Nevertheless, it must be acknowledged that the $\Gamma$ data for $W \geq 0.5$ are quite scattering, especially for $W/D = 0.5$; this scatter could result from both the flapping motion and the estimate method of $\Gamma$ associated with Eq. (1).

The above observations of the approximate linearization for $\Gamma$ are enhanced by those for $\lambda$ and $\eta$, the smaller length scales, see Fig. 10(b) and (c). Namely, better linearities of $\lambda$ and $\eta$ versus $x$ are demonstrated

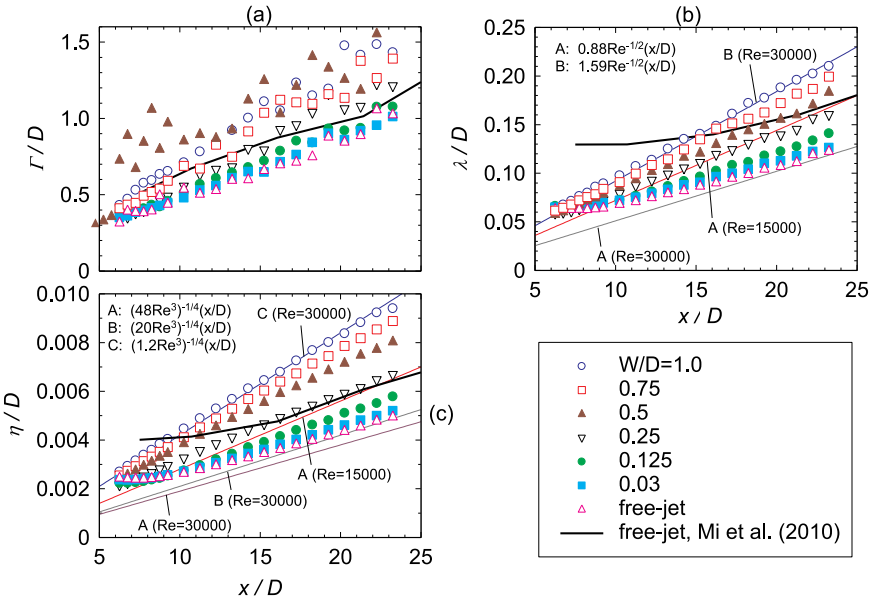


**Fig. 11.** Turbulent integral (Γ), Taylor (λ) and Kolmogorov ($\eta$) scales divided by $D$ along the jet centreline at $Re$ = 30,000 for different widths of the film at $L = D$.

manifestly for all the cases. Nonetheless the effective flow region is seen to increase with increasing $W$. Fig. 11(b) and (c) indeed display that the good linearities of λ and $\eta$ occur at $x/D \geq 6$ for $W \geq 0.5$ and at $x/D \geq 10$ for $W \leq 0.25$ (including the free jet). Worth noting is that λ and $\eta$ from Mi and Nathan (2010) for the free jet ($Re$ = 15,000) are poorly linearized at $x/D \leq 23$. This is expected to result from their hot-wire measurements having much poorer temporal resolutions than the present measurements with the sampling frequency of 50k Hz versus 6k Hz for Mi and Nathan. Their linearized data occur at $x/D \geq 20$, as seen from their Fig. 11. Note that significant differences between the present data and those of Mi and Nathan (2010) derive primarily from different Reynolds numbers ($3.0 \times 10^4$ against $1.5 \times 10^4$).

Of interest, the data scattering of either λ or $\eta$ due to different widths or $x/D$ is substantially smaller than that of Γ. This discrepancy may be attributed to different effects of the flow inlet conditions on large- and small-scale turbulences. It is anticipated that the large-scale turbulence properties should be more sensitive to changes of the inlet and boundary conditions.

Friehe et al. (1972) obtained the following empirical relations for the self-preserving state of the circular free jet:

$$\lambda/D = 0.88\mathrm{Re}^{-1/2}(x/D) \tag{2}$$

and

$$\eta/D = (48\mathrm{Re}^3)^{-1/4}(x/D)\ . \tag{3}$$

Antonia et al. (1980) confirmed Eqs. (2) and (3) by using their hot-wire measurements in several turbulent circular jets. Thirty years later, Mi and Nathan (2010) found that these relations can apply even for the noncircular jets when the pre-factors (0.88, 48) are modified. More recently, Sadeghi and Pollard (2012) made a similar finding for circularly ring-controlled jets. Likewise, the present data of $\lambda/D$ and $\eta/D$ for the free jet agree well with Eqs. (2) and (3).

Highly strikingly, the present results for a set of very different turbulent jets, i.e., the film-flapping jets, also endorse the above findings of Mi and Nathan (2010) and Sadeghi and Pollard (2012). In this context, it is believed that the following relations

$$\lambda/D = a\mathrm{Re}^{-1/2}(x/D) \tag{4}$$

and

$$\eta/D = (b\mathrm{Re}^3)^{-1/4}(x/D) \tag{5}$$

(where $a$ and $b$ are experimental constants depending upon the jet's initial conditions) are widely valid for those turbulent jets which occur naturally or are passively controlled. They may not work for some special jets under active control such as the bifurcating or blooming jets, where the velocity along the nozzle axis can reduce to zero behind the potential core (e.g., Reynolds et al., 2003; Gohil et al., 2015).

In addition, it is impossible for any of the present jets to reach self-preservation at $x/D \leq 23$. For the flapping jets, see Fig. 6, their width is far greater in the flapping plane than in the bisection plane. In other words, the time-averaged field of the flapping jet is cross-sectionally quasi-elliptical even at $x/D$ = 23, far from the asymptotically axisymmetric cross-section. This, from another perspective, implies that the centerline relations (4) and (5) are insensitive to whether the jet has reached self-preservation.

## 4. Conclusions

Our recent work disclosed a new type of flapping jets due to a flexible film fixed at a nozzle exit. The present study has examined the mixing characteristics of the flapping jet of varying film width ($W$) and jet Reynolds number ($Re$). Based on the results reported in Section 3, several key conclusions can be drawn below:

(1) Regarding the film flutter, as $Re$ increases, the flutter frequency grows linearly for $W/D \geq 0.50$, but this linear growth does not hold for $W/D < 0.50$. On the other hand, for any $Re$, as $W$ increases, the flutter frequency grows first and then drops, with the highest value at $W/D = 0.5$.
(2) Regarding the flapping jet, as the film widens, the jet decays and spreads more rapidly. In particular, the decay rate is doubled from $W = 0.25D$ to $W = 0.5D$. Moreover, the near-field turbulence intensity grows with $W$, hence suggesting improved large-scale mixing by widening the film.
(3) The jet flapping motion appears to enhance turbulent mixing at both large and small scales. This is distinct from that of the fluidic nozzle that was found to result in poorly mixing at small scales.
(4) For the present flapping jet, even in the near to intermediate field, the centerline Taylor and Kolmogorov length scales (λ, $\eta$) can well

obey the following relations:

$$\lambda/D = a\mathrm{Re}^{-1/2}(x/D) \text{ and } \eta/D = (b\mathrm{Re}^{3})^{-1/4}(x/D)$$

where the experimental constants $a$ and $b$ depend on the jet-exit conditions. These relations have been also confirmed by experiment to be widely applicable for circular to noncircular free and passively controlled turbulent jets.

## CRediT authorship contribution statement

**M. Wu:** Data curation, Formal analysis, Investigation. **M. Xu:** Conceptualization, Methodology, Software. **J. Mi:** Supervision, Funding acquisition, Writing - original draft. **R.C. Deo:** Software, Validation, Writing - review & editing.

## Declaration of Competing Interest

The authors declare that they have no known competing financial interests or personal relationships that could have appeared to influence the work reported in this paper.

## Acknowledgements

The authors gratefully acknowledge the joint support of the National Key Research and Development Program of China (No. 2016YFB0600605) and National Nature Science Foundation of China (No. 51506019). They also express their gratitude to the two reviewers for their insightful comments on the original manuscript and critical suggestions for the revision.

## Supplementary materials

Supplementary material associated with this article can be found, in the online version, at doi:10.1016/j.ijheatfluidflow.2019.108532.

## References

Antonia, R.A., Satyaprakash, B.R., Hussain, A.K.M.F., 1980). Measurements of dissipation rate and some other characteristics of turbulent plane and circular jets. Phys. Fluids 23 (4), 695–706.
Crow, S.C., Champagne, F.H., 1971. Orderly structure in jet turbulence. J. Fluid Mech. 48, 547–591.
Danaila, I., Boersma, B.J., 2000. Direct numerical simulation of bifurcating jets. Phys. Fluids 12 (5), 1255–1257.
Davis, M.R., 1982. Variable control of jet decay. AIAA J. 20, 606–609.
Friehe, C.A., Van Atta, C.W., Gibson, C.H., 1972). Jet turbulence: dissipation rate measurements and correlations. In: Turbulent Shear Flows, AGARD Conference Proceedings No. 93, p. 18–1.
Glauser, M, Walker, S., 1998. Active flow control to cut millions from jet engine life cycle costs. Air Force Res. Lab. Res. Highlights Sept/Oct 1998.
Gohil, T.B., Saha, A.K., Muralidhar, K., 2015. Simulation of the blooming phenomenon in forced circular jets. J. Fluid Mech. 783, 567–604.
Gutmark, E.J., Grinstein, F.F., 1999. Flow control with noncircular jets. Annu. Rev. Fluid Mech. 31, 239–272.
Hill, W.G., Greene, P.R., 1977. Increased turbulent jet mixing rates obtained by self-excited acoustic oscillations. ASME J. Fluids Eng. 99, 520–525.
Kibens, V, Dorris, J, Smith, DM, Mossman, MF, 1999. Active flow control technology transition: the Boeing ACE program. In: *AIAA 99-3507*. Presented at 30th AAIA Fluid Dyn. Conf. Norfolk, VA.
Manias, C.G., Nathan, G.J., 1993. The precessing jet gas burner − a low $NO_x$ burner providing process efficiency and product quality improvements. World Cement (March) 4–11.
Mi, J., Nathan, G.J., Luxton, R.E., 2001. Mixing characteristics of a flapping jet from a self-exciting nozzle. Flow, Turbul. Combust. 67, 1–23.
Mi J., Nathan G.J., Luxton R.E., 1998. Oscillating jets, PCT/AU98/00959, US Patent No. 6685102 (2004.2), European Pat. No. 1032789 (2004.9).
Mi, J., 2006. Correlation between non-Gaussian statistics of a scalar and its dissipation rate. Phys. Rev. E 74 (1), 016301.
Mi, J., Nathan, G.J., 2010. Statistical properties of turbulent free jets issuing from nine differently-shaped nozzles. Flow Turbul. Combust. 84, 583–606.
Mi, J., Deo, R.C., Nathan, G.J., 2005. Fast-convergent iterative scheme for filtering velocity signals and finding Kolmogorov scales. Phys. Rev. E 71, 066304.
Mungal, M.G., Karasso, P.S., Lozano, A., 1991. The visible structure of turbulent jet diffusion: large-scale organisation and flame tip oscillation. Combust. Sci. Technol. 76, 165–185.
Nathan, G.J., Luxton, R.E., 1991. The entrainment and combustion characteristics and an axisymmetric. self-exciting, enhanced mixing nozzle. ASME/JSME Therm. Eng. Proc. 5, 145–151.
Nathan, G.J., Mi, J., Alwahabi, Z.T., Newbold, G.J.R., Nobe, D.S., 2006. Impacts of a jet's exit flow pattern on mixing and combustion performance. Prog. Energy Combust. Sci. 32, 496–538.
Païdoussis, M.P., 2016. Fluid-Structure Interactions: Slender Structures and Axial Flow 2 Elsevier.
Parekh, D, Leonard, A, Reynolds, W, 1983. A vortex-filament simulation of a bifurcating jet. Bull. Am. Phys. Soc. 28, 1353.
Raman, G., Cornelius, D., 1995. Jet mixing control using excitation from miniature oscillating jets. AIAA J. 33, 365–368.
Reynolds, W.C., Parekh, D.E., Juvet, P.J.D., Lee, M.J.D., 2003. Bifurcating and blooming jets. Annu. Rev. Fluid Mech. 35, 295–315.
Simmons, J.M., Lai, J.C.S., Platzer, M.F., 1981. Jet excitation by an oscillating vane. AIAA J. 19, 673–676.
Sadeghi, H., Pollard, A., 2012. Effects of passive control rings positioned in the shear layer and potential core of a turbulent round jet. Phys. Fluids 24, 115103.
Silva, C.B.d., Métais, O., 2002. Vortex control of bifurcating jets: a numerical study. Phys. Fluids 14 (11), 3798–3819.
Tyliszczak, A., Geurts, B.J., 2014. Parametric analysis of excited round jets – numerical study. Flow, Turbul. Combust. 93, 221–247.
Tyliszczak, A., 2015. LES-CMC of excited hydrogen jet. Combust. Flame 162, 3864–3883.
Viets, H., 1975. Flip-flop jet nozzle. AIAA J. 13, 1375–1379.
Wyngaard, J., 1968. Measurement of small-scale turbulence structure with hot wires. J. Phys. E 1, 1105–1111.
Xu, M., Mi, J., Li, P., 2012. Large eddy simulations of an initially-confined triangular oscillating jet. Flow, Turbul. Combust. 88, 367–386.
Xu, M., Wu, M., Mi, J., 2019. A new type of self-excited flapping jets due to a flexible film at the nozzle exit. Exp. Therm. Fluid Sci. 106, 226–233.